Elastic modulus and its relation to apparent mineral density in juvenile equine bones of the lower limb

Sara G. Moshage[a], Annette M. McCoy[b], Mariana E. Kersh[a,c,d,*]

[a]*Department of Mechanical Science and Engineering, University of Illinois Urbana-Champaign*
[b]*Department of Veterinary Clinical Medicine; University of Illinois Urbana-Champaign*
[c]*Beckman Institute for Advanced Science and Technology; University of Illinois Urbana-Champaign*
[d]*Carle Illinois College of Medicine; University of Illinois Urbana-Champaign*
Urbana, IL, 61801

Abstract

Density-modulus relationships are necessary to develop finite element models of bones that may be used to evaluate local tissue response to different physical activities. It is unknown if juvenile equine trabecular bone may be described by the same density-modulus as adult equine bone, and how the density-modulus relationship varies with anatomical location and loading direction. To answer these questions, trabecular bone cores from the third metacarpal (MC3) and proximal phalanx (P1) bones of juvenile horses (age<1 yr) were machined in the longitudinal (n=134) and transverse (n=90) directions and mechanically tested in compression. Elastic modulus was related to apparent CT density of each sample using power law regressions. We found that density-modulus relationships for juvenile equine trabecular bone were significantly different for each anatomical location (MC3 vs P1) and orientation (longitudinal vs transverse). Use of the incorrect density-modulus relationship resulted in increased root mean squared percent error of the modulus prediction by 8-17%. When our juvenile density-modulus relationship was compared to one of an equivalent location in adult horses, the adult relationship resulted in an 80% increase in error of the modulus prediction. Moving forward, more accurate models of young bone can be developed and used to evaluate potential exercise regimens designed to encourage bone adaptation.

Keywords: juvenile, equine, density, modulus, third metacarpal (MC3), proximal phalanx (P1)

1. Introduction

Limb fractures in horses often result in euthanasia due to limitations of internal fixation related to body mass and anatomy. Up to 80% of racehorse fatalities are caused by a fracture [1], and this number has not improved since the mid-1970s [2]. The majority of fatal musculoskeletal injuries in the lower limb of racing horses occur in the third metacarpus (MC3) and proximal phalanx (P1) [3, 4] and are the result of chronic fatigue [2]. Epidemiological studies have linked several factors to increased fracture risk including racetrack surface, injury history, and sex [1], and significant effort has been placed towards addressing environmental risk factors. While some progress has been made, the goal of preventing essentially all fractures has yet to be realized.

Bone is a functionally adaptive material that responds to its local mechanical environment [5]. Exercise in young horses, while the skeleton is primed for adaptation, has been shown to increase P1 diaphyseal bone mineral content and bone area [6], suggesting an opportunity to direct bone modeling in such a way to reduce fracture risk later in

*Corresponding author
Email address: mkersh@illinois.edu (Mariana E. Kersh)

life. Computational models can be used to non-invasively predict the mechanical loading environment of bone in vivo [7, 8] and therefore provide a means for evaluating the effect of different exercise regimens pre-clinically rather than adopting a trial and error approach. Critical to these predictions is accurate material properties, such as the Young's modulus, which can be related empirically to computed tomography (CT) based apparent mineral density [9, 10].

Several CT density-modulus relationships exist for horse bone [10, 11, 12]. However, the age of the samples ranged from 3-14 years, representing adult bone since equine skeletal maturity occurs at approximately 2 years of age. The most widely used density-modulus relationship for equine bone was developed by Les et al. [10] for longitudinal MC3 samples but the mean sample age was 6.7 years. The non-linear nature of the density-modulus relationship makes it difficult to determine whether one may extrapolate existing functions to young bone. Moreover, structural and compositional differences between juvenile (immature) and adult (mature) bone also motivate the need to consider a different density-modulus relationship for foals than for adult horses.

Like other large mammals, young horses initially have plexiform cortical bone, which contains woven bone, that eventually converts to Haversian bone as they mature [13]. Chappard and colleagues also described juvenile trabecular bone as 'plexiform' but this has not been reported elsewhere [14]. In ovine trabecular bone, mature bone has increased bone volume fraction and apparent ash density, and decreased collagen content when compared to immature bone [15, 16]. Similarly, elastic modulus, ultimate stress, and ultimate strain are known to be different in young bone compared to adult bone [15, 17].

In human trabecular bone it has been established that density-modulus relationships vary by anatomical location [18] and are anisotropic [9], but whether this is true in equine trabecular bone is not known. For example, the growth plates in the distal MC3 and proximal P1 close at the same time [19], however whether or not the bones mineralize at the same rate is not known. Therefore, we hypothesize that juvenile equine bone may require a different density-modulus relationship than those currently reported. Thus, the objective of this study was to develop a density-modulus relationship for juvenile equine bone and evaluate the sensitivity of the density-modulus relationship to anatomical location and loading direction.

2. Materials and Methods

2.1. Specimens

Intact bones (n=18) were collected from young horses euthanized for reasons unrelated to this study (Table 1). Distal limbs were collected within 4 hours of euthanasia and frozen at −20°C. Prior to subsequent steps, distal limbs were cleaned of soft tissue, disarticulated, and the MC3 and P1 were wrapped in PBS soaked gauze and stored in sealed plastic bags at −20°C.

Age (wk)	0.43		4		18		23		48	
Bone	MC3	P1	MC3	P1	MC3	P1	MC3	P1	MC3	P1
Intact Bones	1	1	3	7	1	1	1	1	1	1
Long. Cores	19	3	29	30	12	2	15	9	10	5
Trans. Cores	6	4	19	22	9	2	8	3	12	5

Table 1: Distribution of samples included in this study. Cores were removed in the longitudinal and transverse directions.

2.2. Sample Imaging

The bones and mineral density phantoms (range: 25-750 mg HA/cm^3, CIRS) were scanned in a clinical CT scanner (LightSpeed16, GE Medical Systems) with the same protocols used for live horses (nominal voxel resolution=0.875 x 0.875 x 0.625 mm, 120 kVp, 200 mA). To avoid artifacts (overestimates of apparent CT density) associated with scanning excised cores [20], we developed a method to identify the bone cores virtually within the intact image volume. First, the intact bones were imaged with overlapping microCT (μCT) scans (nominal isotropic resolution = 144 μm, 90 kVp, 177 μA, Rigaku CT-Lab GX130) acquired along the bone length and merged. The intact clinical and μCT scans were aligned in 3D space to share a coordinate system origin and slice plane (Fig. 1A). The bone

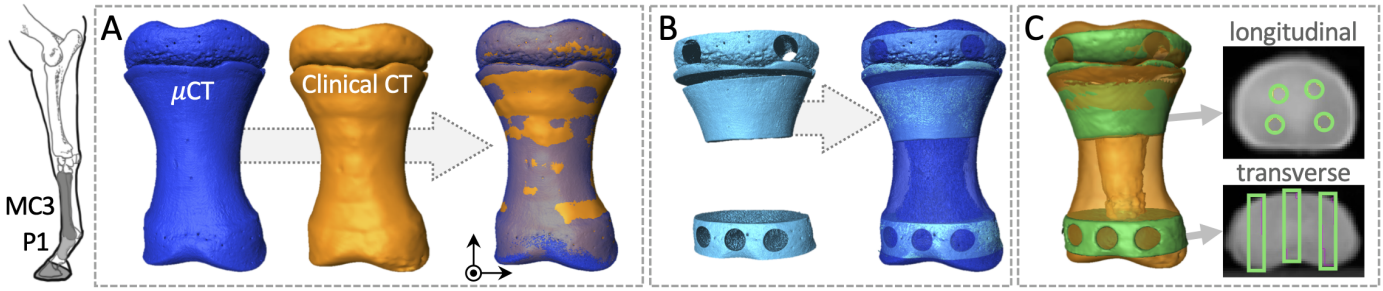

Figure 1: Bone samples were collected from the MC3 and P1 bone of the equine forelimb (far left). (A) Clinical CT scan of a P1 (orange) aligned to whole bone μCT (dark blue) to share a coordinate system origin and slice plane. (B) Bone slabs scanned and aligned to whole bone μCT to locate cores virtually. (C) Bone core location identified within the clinical CT scan and density sampled within the core.

sections that remained following core extraction were μCT scanned and aligned to the intact CT data to locate each core within the μCT data set (Fig. 1B). Virtual location of the cores in the μCT data set were then transformed to the location in the clinical CT data set (Amira 2020.1, Fig. 1C). Custom Matlab code (v2021.b) was then used to separate core CT stacks from the entire bone CT stack via a masking process.

2.3. Bone Core Preparation

In order to maximize the number of cores that could be extracted from each bone, the intact μCT was used to assess the trabecular structure and randomly assign sections of the bone (perpendicular to the long axis) to either longitudinal or transverse cores. Each bone section was cut using a water-irrigated diamond band saw while the bone was frozen. Trabecular cores were removed in the longitudinal (MC3 n=85; P1 n=49) and dorsal-palmar transverse (MC3 n=54; P1 n=36) directions using a water-irrigated diamond sintered coring bit (internal diameter = 5mm) mounted on a drill press. The ends of the cores were trimmed and ground perpendicular to the long axis using sandpaper wetted with PBS (grit: 220, 500, 800). Bone marrow was left intact [21] and the cores were fixed in custom Delrin endcaps using 2-part epoxy (endcap diameter = 19 mm, endcap length $\approx$ 10 mm, exposed length = 12.36$\pm$1.33 mm, total embedded length = 4.83 $\pm$ 1.87 mm). Custom jigs were used during the potting process to ensure the bone sample remained perpendicular to the plane of the endcaps. Between core machining and embedding in endcaps

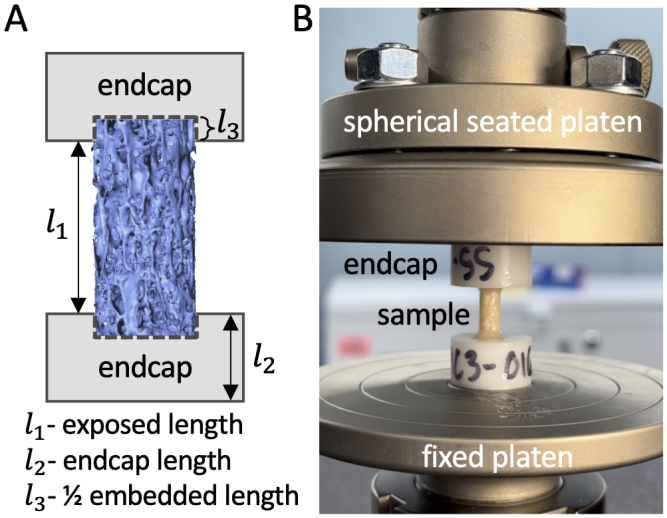

Figure 2: (A) Schematic of sample embedded in Delrin endcaps (dimensions are not to scale). (B) Image of sample in the mechanical test setup.

the samples were wrapped in PBS soaked gauze and stored individually in 5 mL Eppendorf tubes at -20°C. After embedding in endcaps, samples were wrapped in PBS-soaked gauze and refrigerated at approximately 2°C for 18 hours before testing.

2.4. Compression Testing

Cores were returned to room temperature and thoroughly hydrated with PBS. Compression tests were performed on a tabletop test frame (Instron 5967) using a fixed lower platen and a self-aligning, spherical seated upper platen. Embedded cores were pre-loaded to 5N, pre-conditioned for 5 cycles by loading to 0.001 strain at 0.01 strain/s, and then loaded at 0.01 strain/s until failure. Force and crosshead displacement were

recorded after adjusting for machine compliance using the direct technique [22]. Measured displacement was also adjusted to account for endcap material compliance. Force and displacement data were sampled at 100 Hz.

2.5. Young's Modulus Calculation

The diameter and the exposed length of each core was measured using digital calipers. Stress was calculated by dividing force by each sample's cross-sectional area (diameter=4.97±0.04mm). Strain was calculated by dividing displacement by effective gauge length (exposed length + 1/2 length embedded in endcaps [23]) of each sample. Young's modulus was calculated as the slope of the linear regression of all data between two points on the elastic portion (approximately 0.003-0.018 ε) of the stress-strain curve.

2.6. Density measurement and density-modulus relationship

The clinical CT scan and phantoms were used to calculate average CT density (ρ_{CT}, g HA/cm^3) for each core. Modulus and CT density data were pooled by bone type (MC3, P1) and orientation of core (longitudinal, transverse). In order to satisfy the assumptions of linearity, homoscedasticity, and normality of residuals, modulus and CT density were both log transformed. We used a linear mixed effects regression between modulus (dependent variable) and CT density (fixed effect), with subject included as a random effect (random intercept). The slope and intercept were used to define the exponential and leading coefficient terms, respectively, in the function relating modulus to CT density.

2.7. Statistical Analysis

Normality of Young's modulus within each bone and anatomical location was evaluated using a Shapiro-Wilks test. Modulus in the MC3 longitudinal and transverse directions and P1 longitudinal direction were not normally distributed; therefore, distributions were compared between all groups using a Mann-Whitney-Wilcoxon test. To assess the effect of anatomical location and loading direction on the density-modulus relationship, additional models were created with those variables as fixed effects, allowing for interaction with CT density, and compared to a model without the variable in question via likelihood ratio test to obtain a p-value. Linear mixed effects models do not have an R^2 in the traditional sense, therefore the method defined by Nakagawa and Schielzeth was used to calculate a marginal R^2 that represents the variance explained by the fixed factors (CT density) [24]. All analyses were performed in R (v4.2.1) and the *lme4* package was used to perform the linear mixed effects analysis.

3. Results

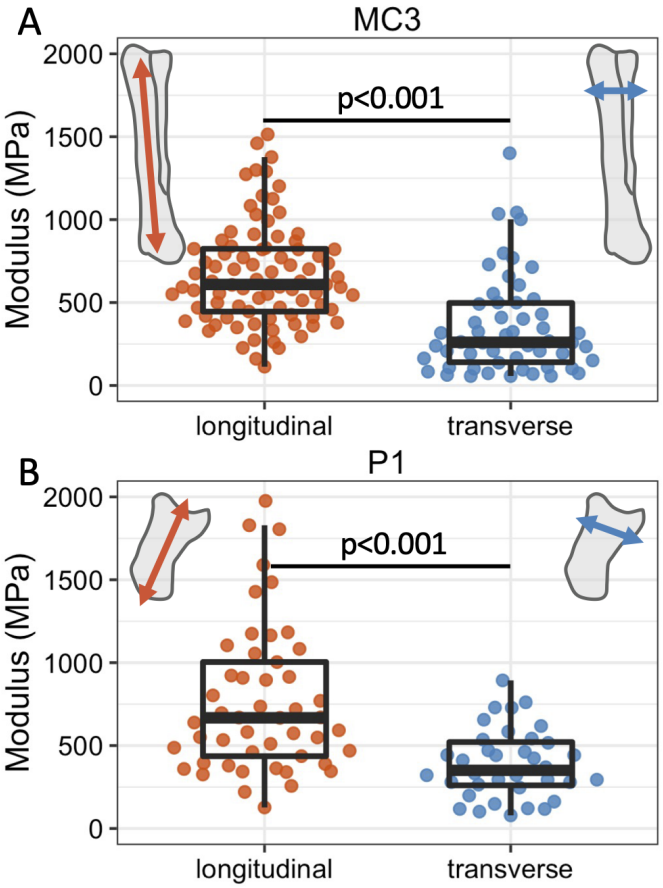

Figure 3: Young's modulus for the (A) MC3 and (B) P1 samples in the longitudinal (orange) and transverse (blue) directions. Distributions of modulus were significantly different between orientations within a bone, but not between bones.

All data are presented as median±median absolute deviation. Of the Young's modulus data

shown in Fig. 3, only the P1 transverse data was normally distributed. The longitudinal modulus was 134% higher than the transverse modulus in the MC3 (Fig. 3A) and 90% higher in the P1 (Fig. 3B); these distributions differed significantly ($p<0.001$ for both). The transverse modulus of MC3 samples was lower (260±230 MPa) than the P1 (351±202 MPa, Fig. 3), although these distributions did not differ significantly ($p=0.12$). There was no significant difference between longitudinal samples from the MC3 and P1 (609±297 MPa and 667±405 MPa, respectively).

Within the MC3 samples, orientation significantly affected model predictions of modulus ($p<0.001$), indicating that the longitudinal and transverse directions should have separate equations. When all P1 data were pooled, orientation significantly affected the model ($p<0.001$), again indicating models should be orientation specific. When data were pooled for each direction and anatomical location was included as a fixed effect, location significantly affected the model ($p<0.001$ in the longitudinal direction, $p=0.02$ in the transverse direction). Together, these model results indicate that each anatomical location and orientation requires a different density-modulus relationship (Fig. 4).

Overall, the transverse modulus was better predicted than longitudinal modulus in both bones, with CT density predicting 86% of the variability in the P1 and 77% of the variability in the MC3 (Fig. 4, blue lines). Variability in the longitudinal modulus was similarly predicted in both bones (R^2=0.62 in MC3, R^2=0.66 in P1). Root mean squared percent error (RMSPE) was calculated for each of the density-modulus relationships to assess the magnitude of error in relation to actual values. In the MC3 (Fig. 4A), RMSPE was 35% in the longitudinal direction and 45% in the transverse direction. In the P1 (Fig. 4B), RMSPE was 32% in the longitudinal direction and 23% in the transverse direction.

4. Discussion

Using a robust sample size, we have developed the first density-modulus relationships for the juvenile equine MC3 and P1. To evaluate whether indeed this relationship is different from those derived from older bone, we compared our juvenile longitudinal MC3 data to that reported by Les et al [10]. Apparent CT density was converted to ash density (ρ_{ash} (g/cm^3), Eq. 1 [25]) and ash

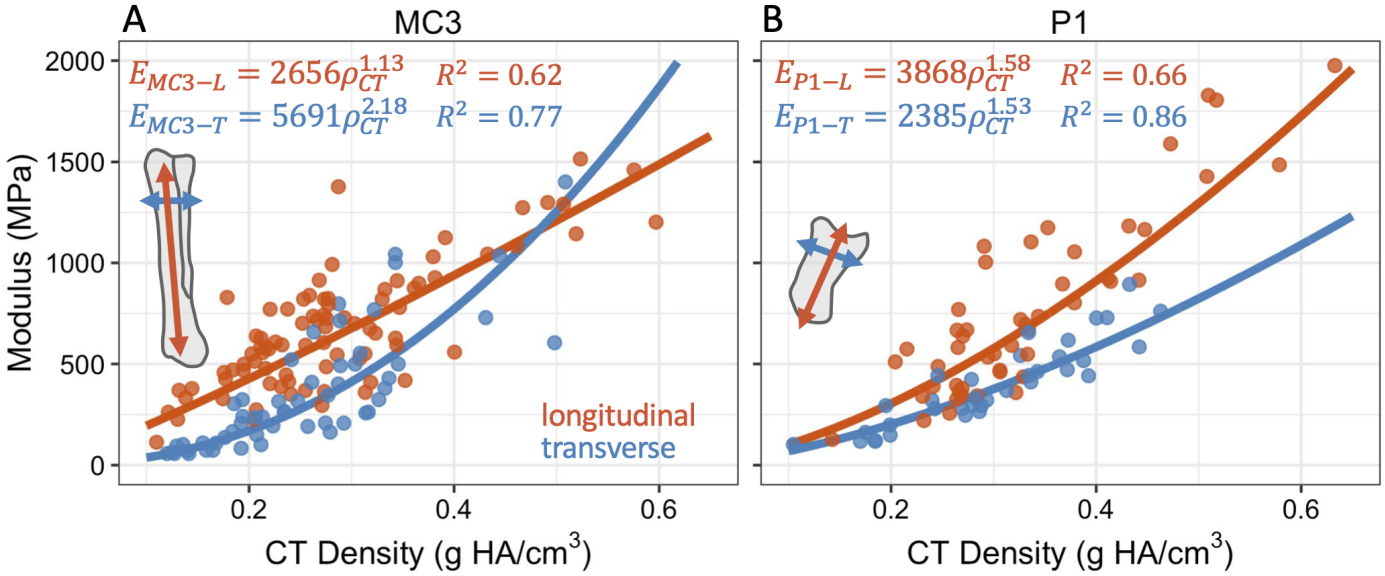

Figure 4: Density-modulus relationships for the (A) MC3 and (B) P1 samples in the longitudinal (orange) and transverse (blue) directions. Printed R^2 values are marginal R^2 values, which measures the variance in modulus that can be explained by CT density. In each of these relationships, subject (donor of the bone samples) was included as a random effect.

density-modulus relationships were calculated.

$$\rho_{ash} = (\rho_{CT} + 0.09)/1.14 \quad (1)$$

The root mean squared error (RMSE) was 347 MPa using E_{adult}, which is almost 80% higher than the RMSE when using the model developed here for juvenile bone, E_{young} (191 MPa) (Fig. 5). Modulus values for adult MC3 trabecular bone in compression range from 2.09-3.65 GPa [11, 12, 26], while median modulus for our juvenile MC3 longitudinal samples was 609±297 MPa. It should be noted that over 80% of the samples tested by Les et al. were cortical bone (although they reported no difference in the density-modulus relationship between cortical and trabecular bone [10]), while our samples were trabecular. Bone volume fraction in the distal MC3 condyles reportedly increases from approximately 32% in 1-2 month old horses to approximately 60% in horses greater than 6 years old [27]. As apparent CT density is a combined measure of bone volume fraction and tissue density, it is expected that apparent CT density changes with maturation.

While differences in intrinsic properties between immature and mature bone are the most likely explanations for why density-modulus relationships differ with age, there are also methodological differences in the measurement of Young's modulus that are worth mentioning. We tested our samples using endcaps while Les et al. tested samples in compression using platens directly in contact with the bone sample, which has since been shown to result in an underestimation of modulus by 20-40% [23] in trabecular bone samples. The underestimation of modulus would likely cause an even larger disparity between the density-modulus developed here for juvenile bone than that reported for older bone but this remains to be confirmed.

We found that density-modulus relationships in juvenile equine trabecular bone vary depending on anatomical location (MC3 vs P1) and loading direction (longitudinal vs transverse), which is consistent with human data [18, 9]. The impact of not accounting for differences between bones

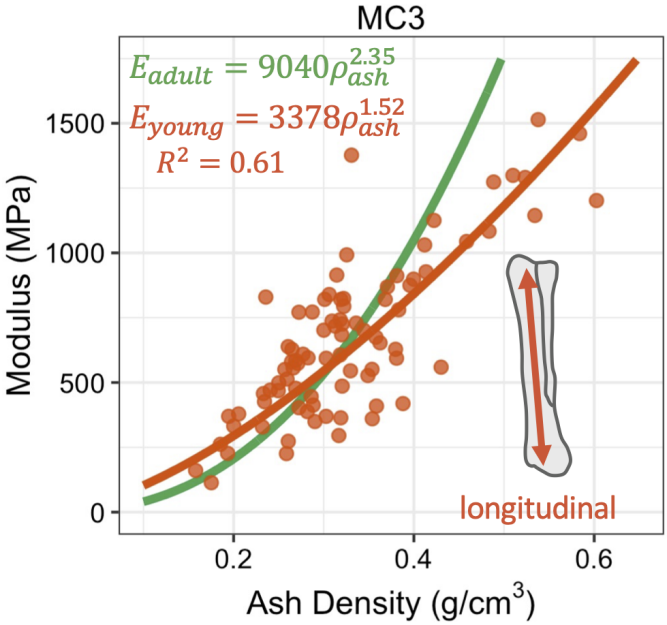

Figure 5: Density-modulus relationships for the MC3 comparing adult (E_{adult} [10]) and juvenile (E_{young}) samples.

when predicting modulus from CT data is notable. Applying the MC3 density-modulus relationships to the P1 data results in an RMSPE of 49% in the longitudinal direction and 31% in the transverse direction, which are both higher than the percent error obtained with using the P1 density-modulus relationships (longitudinal: 32%, transverse: 23%).

There are several reasons why the density-modulus relationships between bones may be different. Biomechanically, the two bones are likely under different types of loads with the MC3 in combined bending and compression due to its long slender structure and distribution of cortical material properties [28]. In contrast, the cuboidal P1 would be more resistant to bending. Variation in surface strain modes between the distal MC3 (compression) and the P1 (shear) have been reported [29, 30].

We also found that the density-modulus relationships in the transverse direction had stronger predictions of modulus than the longitudinal direction (Fig. 4). The density-modulus relationship of the P1 in the transverse direction (E_{P1-T}) had the highest R^2 (0.86) and lowest percent error (RMSPE=23%) of all relationships investigated.

The density-modulus relationship of the MC3 in the transverse direction (E_{MC3-T}) also had a high R^2 (0.77) but had the highest percent error (RMSPE=45%) of all relationships, which was driven by increased variability of the modulus data between a CT density of 0.2-0.5 g HA/cm^3. For example, at a density of approximately 0.28 g HA/cm^3 in the MC3 (Fig. 4A), the transverse modulus ranges from approximately 200-800 MPa (blue data).

The sensitivity of the strength of modulus predictions to orientation may be related to the nature of the microstructure along each direction. Longitudinal cores tend to have more varied microstructure along the length of the sample (Fig. 6A) when compared to the more compact microstructure evident in transverse cores (Fig. 6B). However, these microstructural differences may be unique to juvenile animals, as Keyak et al. reported similar R^2 values in density-modulus relationships for adult human proximal tibia bone in the longitudinal (0.84) and transverse directions (anterior-posterior: 0.72; medial-lateral: 0.84) [9]. Augat et al. found approximately equivalent coefficient of variation in modulus between the longitudinal and both transverse directions of adult human trabecular bone in the spine, calcaneus, proximal femur, and distal femur [31]. Further work is needed to confirm whether mineralization rates are different between the MC3 and P1, as well as the influence of microstructure and tissue mineral density on the elastic modulus.

Although a driving motivator for this study was the ability to more accurately evaluate the mechanical environment during exercise in juvenile horses, there are other applications. Finite element models based on CT data have been used to assess fracture risk and represent an improved assessment of bone strength when compared to densitometric variables alone [32]. Finite element models can also be used as a pre-surgical evaluation tool to predict tissue response to certain fixation methods [33]. Use of the incorrect density-modulus relationship may result in incorrect assessments of bone strength or pre-surgical evaluation, therefore, our findings may have direct clinical implications.

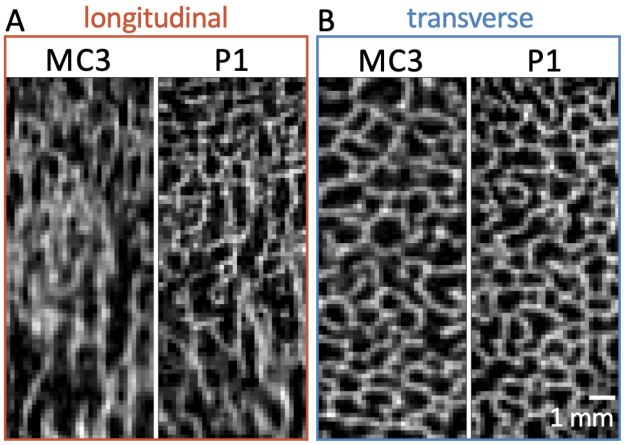

Figure 6: MicroCT images of representative cores in the (A) longitudinal and (B) transverse directions of the MC3 and P1, from the same subject. All images are at nominal isotropic resolution of 144 μm. Scale bar is equivalent for all images.

There are several limitations of this study. Transverse bone samples were only machined in the dorsal-palmar ("anterior-posterior") direction. The geometry of the MC3 and P1 led to challenges in excising cores in the medial-lateral direction, and limited availability of intact juvenile bones required we waste as little tissue as possible. The implications of this may be mitigated by the fact that trabecular bone has been described as a transversely isotropic structure [34], and modulus values in the anterior-posterior and medial-lateral directions often have a similar relationship with ash density [9] and bone volume fraction [35]. Despite the fact that we tested over 200 samples, we still encountered variability in the density-modulus data that leaves over 30% of the modulus variability unexplained in the case of the longitudinal MC3 (Fig. 4A, E_{MC3-L}). Aside from the influence of microstructure on mechanical properties, some of this variability may be due to sample age, as we had donors ranging in age from approximately 0.5 week to 48 weeks. As well, 35% of samples in the MC3 and 60% of samples in the P1 (combining both orientations) were from subjects that were 4 weeks old. Sample size in the current study does not allow us to develop statistically meaningful density-modulus relationships for each age of juvenile horses, and instead data were pooled to describe horses less than 1

year old. Nonetheless, all model predictions were significant and this work represents the first large scale mechanical testing study in juvenile equine bone.

Therefore, using rigorous imaging and experimental protocols, we have established orientation-specific density-modulus relationships for the juvenile MC3 and P1 bones. The incorporation of these data into computational models will allow for more accurate predictions of the mechanical response of young bone to loads and therefore the potential for bone adaptation.

5. Conflict of Interest

None

6. Acknowledgements

Samples were collected by AMM during 2018-2022 from patients requiring euthanasia at the Large Animal Clinic of the Veterinary Teaching Hospital at UIUC. We are grateful for the technical support from Dr. Leilei Yin for his help with μCT scanning, and to the Visualization Laboratory at the Beckman Institute for Advanced Science and Technology for providing software used in this project. Funding was provided by USDA Hatch Funds (ILLU-888-964), Campus Research Board at UIUC, Grayson Jockey Club Research Foundation, and a graduate fellowship from the Beckman Institute for Advanced Science and Technology to SGM.

7. Nomenclature

CT - computed tomography
E - density-modulus relationship
MC3 - third metacarpal
P1 - proximal phalanx

Greek Letters

μ - micro
ρ - density, g/cm^3

Subscripts

adult - data from Les et al. [10]
ash - relating to amount of mineral, indicating ash density
CT - from clinical CT, indicating apparent CT density
MC3-L - from the MC3 bone in the longitudinal direction
MC3-T - from the MC3 bone in the transverse direction
P1-L - from the P1 bone in the longitudinal direction
P1-T - from the P1 bone in the transverse direction
young - juvenile MC3 data in the longitudinal direction

References

[1] S. P. Georgopoulos, T. D. Parkin, Risk factors for equine fractures in Thoroughbred flat racing in North America, Preventive Veterinary Medicine 139 (2017) 99–104. doi:10.1016/j.prevetmed.2016.12.006.

[2] C. M. Riggs, Fractures - A preventable hazard of racing thoroughbreds?, The Veterinary Journal 163 (1) (2002) 19–29. doi:10.1053/tvjl.2001.0610.

[3] K. Verheyen, J. Wood, Descriptive epidemiology of fractures occurring in British Thoroughbred racehorses in training, Equine Veterinary Journal 36 (2) (2004) 167–173. doi:10.2746/0425164044868684.

[4] A. Bertuglia, M. Bullone, F. Rossotto, M. Gasparini, Epidemiology of musculoskeletal injuries in a population of harness Standardbred racehorses in training, BMC Veterinary Research (2014). doi:10.1186/1746-6148-10-11.

[5] P. Pivonka (Ed.), Multiscale Mechanobiology of Bone Remodeling and Adaptation, Vol. 578 of CISM International Centre for Mechanical Sciences, Springer International Publishing, Cham, Switzerland, 2018. doi:10.1007/978-3-319-58845-2.

[6] E. C. Firth, C. W. Rogers, P. R. van Weeren, A. Barneveld, C. W. McIlwraith, C. E. Kawcak, A. E. Goodship, R. K. Smith, Mild exercise early in life produces changes in bone size and strength but not density in proximal phalangeal, third metacarpal and third carpal bones of foals, The Veterinary Journal 190 (3) (2011) 383–389. doi:10.1016/j.tvjl.2010.11.016.

[7] M. E. Kersh, S. Martelli, R. Zebaze, E. Seeman, M. G. Pandy, Mechanical loading of the femoral neck in human locomotion, Journal of Bone and Mineral Research 33 (11) (2018) 1999–2006. doi:10.1002/jbmr.3529.

[8] C. Yan, R. J. Bice, J. W. Frame, S. J. Warden, M. E. Kersh, Multidirectional basketball activities load different regions of the tibia: A subject-specific muscle-driven finite element study, Bone 159 (2022) 116392. doi:10.1016/j.bone.2022.116392.

[9] J. Keyak, I. Lee, H. Skinner, Correlations between orthogonal mechanical properties and density of trabecular bone, Journal of Biomedical Materials Research 28 (1994) 1329–1336. doi:10.1002/jbm.820281111.

[10] C. M. Les, J. H. Keyak, S. M. Stover, K. T. Taylor, A. J. Kaneps, Estimation of material properties in the equine metacarpus with use of quantitative computed tomography, Journal of Orthopaedic Research 12 (6) (1994) 822–833. doi:10.1002/jor.1100120610.

[11] P. D. Leahy, B. S. Smith, K. L. Easton, C. E. Kawcak, J. C. Eickhoff, S. S. Shetye, C. M. Puttlitz, Correlation of mechanical properties within the equine third metacarpal with trabecular bending and multi-density micro-computed tomography data, Bone 46 (2010) 1108–1113. doi:10.1016/j.bone.2010.01.366.

[12] J. Symons, R. Entwistle, A. Arens, T. Garcia, B. Christiansen, D. Fyhrie, S. Stover, Mechanical and morphological properties of trabecular bone samples obtained from third metacarpal bones of cadavers of horses with bone fragility syndrome and horses unaffected by that syndrome, American Journal of Veterinary Research 73 (11) (2012) 1742–1751. doi:10.2460/ajvr.73.11.1742.

[13] M. L. Hillier, L. S. Bell, Differentiating human bone from animal bone: A review of histological methods, Journal of Forensic Sciences 52 (2) (2007) 249–263. doi:10.1111/j.1556-4029.2006.00368.x.

[14] D. Chappard, M.-F. Baslé, E. Legrand, M. Audran, Trabecular bone microarchitecture: A review, Morphologie 92 (299) (2008) 162–170. doi:10.1016/j.morpho.2008.10.003.

[15] A. Nafei, C. C. Danielsen, F. Linde, I. Hvid, Properties of growing trabecular ovine bone - Part 1: Mechanical and physical properties, The Journal of Bone and Joint Surgery 82 (6) (2000) 11. doi:10.1302/0301-620X.82B6.0820910.

[16] A. Nafei, J. Kabel, A. Odgaard, F. Linde, I. Hvid, Properties of growing trabecular ovine bone - Part 2: Architecural and mechanical properties, The Journal of Bone and Joint Surgery 82 (6) (2000) 7. doi:10.1302/0301-620X.82B6.0820921.

[17] M. Ding, M. Dalstra, C. Danielsen, J. Kabel, I. Hvid, F. Linde, Age variations in the properties of human tibial trabecular bone, Journal of Bone Joint Surgery 79 (6) (1997) 995–1002. doi:10.1080/17453674.2000.11744841.

[18] E. F. Morgan, H. H. Bayraktar, T. M. Keaveny, Trabecular bone modulus-density relationships depend on anatomic site, Journal of Biomechanics 36 (7) (2003) 897–904. doi:10.1016/S0021-9290(03)00071-X.

[19] J. E. Smallwood, S. M. Albright, M. R. Metcalf, D. E. Thrall, B. D. Harrington, A xeroradiographic study of the developing equine foredigit and metacarpophalangeal region from birth to six months of age, Veterinary Radiology 30 (3) (1989) 98–110. doi:10.1111/j.1740-8261.1989.tb00753.x.

[20] M. G. Drum, C. M. Les, R. D. Park, C. W. McIlwraith, C. E. Kawcak, Comparison of mean bone densities of three preparations of the distal portion of the equine third metacarpal bone measured by use of quantitative computed tomography, American Journal of Veterinary Research 69 (7) (2008) 891–893. doi:10.2460/ajvr.69.7.891.

[21] S. Zhao, M. Arnold, R. L. Abel, J. P. Cobb, S. Ma, U. Hansen, O. Boughton, Standardizing Compression Testing for Measuring the Stiffness of Human Bone, Bone and Joint Research 7 (8) (2018) 524–538. doi:10.1302/2046-3758.78.BJR-2018-0025.R1.

[22] S. R. Kalidindi, A. Abusafieh, E. El-Danaf, Accurate characterization of machine compliance for simple compression testing, Experimental Mechanics 37 (2) (1997) 210–215. doi:10.1007/BF02317861.

[23] T. M. Keaveny, T. P. Pinilla, R. P. Crawford, D. L. Kopperdahl, A. Lou, Systematic and random errors in compression testing of trabecular bone, Journal of Orthopaedic Research 15 (1) (1997) 101–110. doi:10.1002/jor.1100150115.

[24] S. Nakagawa, H. Schielzeth, A general and simple method for obtaining R^2 from generalized linear mixed-effects models, Methods in Ecology and Evolution 4 (2) (2013) 133–142. doi:10.1111/j.2041-210x.2012.00261.x.

[25] E. Schileo, E. Dall'Ara, F. Taddei, A. Malandrino, T. Schotkamp, M. Baleani, M. Viceconti, An accurate estimation of bone density improves the accuracy of subject-specific finite element models, Journal of Biomechanics 41 (11) (2008) 2483–2491. doi:10.1016/j.jbiomech.2008.05.017.

[26] S. Martig, P. V. S. Lee, G. A. Anderson, R. C. Whitton, Compressive fatigue life of subchondral bone of the metacarpal condyle in thoroughbred racehorses, Bone 57 (2) (2013) 392–398. doi:10.1016/j.bone.2013.09.006.

[27] N. Anne-Archard, G. Martel, U. Fogarty, H. Richard, G. Beauchamp, S. Laverty, Differences in third metacarpal trabecular microarchitecture between the parasagittal groove and condyle at birth and in adult racehorses, Equine Veterinary Journal 51 (2019) 115–122. doi:10.1111/evj.12980.

[28] C. M. Les, S. M. Stover, J. H. Keyak, K. T. Taylor, N. H. Willits, The distribution of material properties in the equine third metacarpal bone serves to enhance sagittal bending, Journal of Biomechanics (1997). doi:10.1016/S0021-9290(96)00157-1.

[29] J. S. Merritt, M. G. Pandy, N. A. Brown, C. R.

Burvill, C. E. Kawcak, C. W. McIlwraith, H. M. Davies, Mechanical loading of the distal end of the third metacarpal bone in horses during walking and trotting, American Journal of Veterinary Research 71 (5) (2010) 508–514. doi:10.2460/ajvr.71.5.508.

[30] E. Singer, T. Garcia, S. Stover, How does bone strain vary between the third metacarpal and the proximal phalangeal bones of the equine distal limb?, Journal of Biomechanics 123 (2021) 110455. doi:10.1016/j.jbiomech.2021.110455.

[31] P. Augat, T. Link, T. F. Lang, J. C. Lin, S. Majumdar, H. K. Genant, Anisotropy of the elastic modulus of trabecular bone specimens from different anatomical locations, Medical Engineering & Physics 20 (2) (1998) 124–131. doi:10.1016/S1350-4533(98)00001-0.

[32] P. K. Zysset, E. Dall'Ara, P. Varga, D. H. Pahr, Finite element analysis for prediction of bone strength, BoneKEy Reports 2 (Aug. 2013). doi:10.1038/bonekey.2013.120.

[33] L. L. Frazer, E. M. Santschi, K. J. Fischer, Stimulation of subchondral bone cyst healing by placement of a transcondylar screw in the equine medial femoral condyle, Veterinary Surgery 48 (7) (2019) 1194–1203. doi:10.1111/vsu.13247.

[34] A. Odgaard, J. Kabel, B. van Rietbergen, M. Dalstra, R. Huiskes, Fabric and elastic principal directions of cancellous bone are closely related, Journal of Biomechanics 30 (5) (1997) 487–495. doi:10.1016/S0021-9290(96)00177-7.

[35] B. van Rietbergen, R. Huiskes, Elastic constants of cancellous bone, in: Bone Mechanics Handbook, 2nd Edition, 2009, pp. 15–1:15–24.

Figures and tables

Table 1: Distribution of samples included in this study. Cores were removed in the longitudinal and transverse directions.

Figure 1: (Bone samples were collected from the MC3 and P1 bone of the equine forelimb (far left). (A) Clinical CT scan of a P1 (orange) aligned to whole bone μCT (dark blue) to share a coordinate system origin and slice plane. (B) Bone slabs scanned and aligned to whole bone μCT to locate cores virtually. (C) Bone core location identified within the clinical CT scan and density sampled within the core.

Figure 2: (A) Schematic of sample embedded in Delrin endcaps (dimensions are not to scale). (B) Image of sample in the mechanical test setup.

Figure 3: Young's modulus for the (A) MC3 and (B) P1 samples in the longitudinal (orange) and transverse (blue) directions. Distributions of modulus were significantly different between orientations within a bone, but not between bones.

Figure 4: Density-modulus relationships for the (A) MC3 and (B) P1 samples in the longitudinal (orange) and transverse (blue) directions. Printed R^2 values are marginal R^2 values, which measures the variance in modulus that can be explained by CT density. In each of these relationships, subject (donor of the bone samples) was included as a random effect.

Figure 5: Density-modulus relationships for the MC3 comparing adult (E_{adult} [10]) and juvenile (E_{young}) samples.

Figure 6: MicroCT images of representative cores in the (A) longitudinal and (B) transverse directions of the MC3 and P1, from the same subject. All images are at nominal isotropic resolution of 144 μm. Scale bar is equivalent for all images.